

Endothelial proliferation modulates neuron-glia survival and differentiation in ischemic stress

Ogundele O Michael¹, Balogun W Gbolahan², Cobham E Ansa², Amin Abdulbasitand³, Ishola O Azeez²

¹Department of Anatomy, College of Medicine and Health Sciences, AfeBabalola University, Ekiti State Ado-Ekiti, Nigeria; ²Department of Anatomy, College of Health Sciences, University of Ilorin, Ilorin, Kwara State, Nigeria; ³Department of Physiology, College of Health Sciences, University of Ilorin, Ilorin, Kwara State, Nigeria

KEY WORDS

Cyanide
Ischemia
Vascular occlusion
Oxidative stress
Stroke
Glia
Endothelium
Blood vessel

ABSTRACT

Background: Recent studies have shown that endothelial proliferation and angiogenic response are characteristic of degenerative events, such that the magnitude of endothelial activation is reflective of the progression of neurodegeneration.

Purpose: This study sets out to, compare, the degenerative changes seen in the parietal cortex (PC) and periventricular zone (PVZ) after cyanide toxicity or vascular occlusion.

Methods: Global vascular occlusion (VO) and cyanide toxicity (CN) were induced in separate sets of male adult wistar rats for 10 days (treatment phase). Subsequently, the treatment was discontinued for another 10 days (withdrawal phase) (CN-I and VO-I). A separate group of control was maintained for 10 days and received normal saline for this duration. The animals were euthanized at day 10 (treatment and control) and day 20 (withdrawal) after which the tissue was processed for antigen retrieval immunohistochemistry to demonstrate; H&E (general histology) CD31/PECAM 1(endothelial proliferation), CD45 (monocyte/phagocyte), GFAP (glia), NSE (neuron), Ki-67 (cell proliferation) and NF (neurofilament). Total cell count, immunopositive cell counts, arterial wall thickness and lumen width were determined and plotted using ANOVA with significance set at $P < 0.05^*$.

Result: We observed an increase in endothelial proliferation (\uparrow CD31), glia activation and a decrease in neuron count in vascular occlusion and cyanide toxicity after the treatment phase (degeneration). The neuron count increased (\uparrow NSE) after withdrawal of cyanide treatment and vascular occlusion and was accompanied by a corresponding decrease in endothelial and glia activation (\downarrow CD31/GFAP). Degenerative changes were more prominent in cyanide toxicity when compared with vascular occlusion. The increase in CD45 expression coupled with a reduced CD31/GFAP after the withdrawal phase was evident of vascular remodeling and neurosurvival.

Conclusion: We conclude that neuronal degeneration in cyanide toxicity or vascular occlusion is dependent on an increase in endothelial proliferation (\uparrow CD31), glia activation (\uparrow GFAP) and a decrease in monocyte expression (\downarrow CD45); representing a pro-inflammatory response. Furthermore, cyanide toxicity induced more prominent degenerative changes when compared with the vascular occlusion due to a higher CD31/GFAP expression. Subsequent withdrawal of the ischemia facilitated a reduction in GFAP/CD31 with a corresponding increase in monocytes (\uparrow CD45) for vascular remodeling and neurosurvival. The VO-I showed a significant increase in vascular remodelling than the CN-I due to a more significant increase in monocytic expression (CD45) after the withdrawal of the occlusion. Generally, we found that degeneration was prominent in the parietal cortex and less in the periventricular zone for both forms of ischemia.

doi : 10.5214/ans.0972.7531.220305

Corresponding Author:

Ogundele O Michael
Tel : +2347031022702
E-mail : ola.ogundele@abuad.edu.ng



Olalekan M. Ogundele

Introduction

Cellular and cardiovascular incidents are important aspects of ischemic injuries observed in stroke and other related cerebrovascular disorders.¹ Although oxygen deprivation at cellular level is associated with vascular occlusion and cyanide neurotoxicity (mitochondrial poisoning), the

symptoms exhibited in the patients differ to a certain extent.^{2,3} In vascular occlusion, the symptoms are usually rapid and severe; in most cases involving partial or full paralysis while cyanide toxicity causes neurological disorders (degenerative) over a period of time, depending on the dosage and

the duration of exposure. The common set of events in cyanide toxicity and vascular occlusion involves inflammatory and degenerative cascades starting from oxygen deprivation and ending in cell death.^{4,5} Furthermore, metabolic changes induced in this cascade are a reflection of dysregulated mitochondria and extrinsic signaling pathways that leads to production of reactive oxygen species (ROS), reactive nitrogen species (RNS) and nitric oxide (NO). These alterations in metabolic and cellular processes also involve changes in the morphology of the cerebral blood vessels and blood flow pattern in the affected brain regions.^{5,6}

The blood supply of the brain is intriguing as the large arteries are connected by vast anastomotic network that dis-

tributes blood to the neural tissue through its terminal “end arteries”.^{7,8} The end arteries exist at the capillary level of cerebral circulation and are single cell thick with an underlying endothelium forming a structural part of the blood brain barrier (BBB) unit.^{5,8} Ultramicroscopic.^{5,8} Ultramicroscopic analysis of the structure of a single BBB unit reveals that the endothelial cells of the end arteries are linked via intercellular junctions to the ependymal astrocytes and tanycytes occupying the immediate surroundings of the arteries.⁹ The matrix rich endothelium (charged molecules), surrounding astrocytes, neurons and blood cells form the structural, physiological and electrical barrier that controls the bi-directional movement of molecules across the blood-brain interphase.⁴ The significance of such bi-directional flow has been described as regulatory as it is involved in homeostatic efficiency of regional circulation and metabolism in the central nervous system (CNS).^{4,10}

The importance of the endothelium as an integral part of the BBB has been emphasized. Previous studies have shown, using high magnification microscopy, that endothelial cells provide structural and physiological barrier at the interphase of neuron/glia and the circulating blood; such that toxins, nutrients, microbes, viruses and metabolites in the blood come in contact with the endothelium before the cells of the nervous system.^{11,8} Proliferative or degenerative changes in the endothelium have been linked with the progression of most degenerative diseases. This may involve changes in endothelial cells, adhesion molecules and matrix and is often the cause in brain infections, chemotoxicity and inflammation.¹²

Recent studies have shown that bi-directional signals across the BBB actively modulate the pathophysiological process of degeneration in stroke, chemotoxicity and acute brain injuries.^{4,11,13} An example of such cellular signal is the “danger associated molecular pattern (DAMP)” associated with the release of chemokines and cytokines into the blood after traumatic brain injury. As a result, a more robust immune response, resulting in inflammation is activated.^{13,14} Interestingly, other studies have shown that the bi-directional communication between the ischemic or inflamed nervous system and the cells of the endothelium regulate the DAMP signal, and thus the progression of brain injuries.^{10,15,16}

Differential cellular mechanisms are involved in the progression of endothelial and neural changes induced by chemotoxicity and vascular occlusion.^{17–20} Although a common factor in the progression of these models is oxidative stress, the pattern of endothelial/angiogenic response and how it affects the progression of degeneration and neurosurvival is yet to be elucidated. Generally, the induced oxidative stress has been described as a trigger of neuronal cell death, endothelial proliferation, glia activation, inflammation and in some cases proliferation in specific brain regions.^{15,16,21–24} In addition, our previous findings of glia activation, neuronal degeneration and proliferation induced by differential oxidative stress has revealed that regional differences exist in stress response elicited in the brain; specifically across the plastic and non-plastic brain regions.²⁵

Consequently, we investigated the effects of cyanide toxicity and vascular occlusion on the endothelial (CD31/CD45), neuron (NSE) and glia (GFAP) cells using immunohistochemistry and stereology in cortical slices. We compared the effect of cyanide toxicity and

vascular occlusion in the plastic periventricular zone (PVZ) and non-plastic parietal cortex (PC) in order to detect either proliferation (Ki-67) or degeneration (NF) relative to endothelial changes (CD31/CD45) after the treatment and withdrawal phases. Our findings demonstrate that endothelial changes are linked with glia activation, neuronal degeneration and proliferation. In addition, the observed changes vary for cyanide toxicity and vascular occlusion after the treatment and withdrawal periods.

Methods

Treatment

$N = 30$ male adult Wistar rats, weighing between (250–280 gms) were used for this study. A group of $n = 12$ rats were treated with orally administered potassium cyanide (KCN) (30 mg/Kg body weight (BW) for 10 days using a gavage (CN).^{26–28} A separate set of $n = 12$ animals was subjected to transient occlusion of carotid arteries, basilar artery and brachiocephalic vein using an elastic neck cuff. This was accompanied by a reduction of blood pressure above the neck cuff to 30 mmHg (VO).^{29–32} The control (CO; $n = 6$) received normal saline for the total duration of the treatment phase (10 days). At the end of the treatment phase, $n = 6$ animals were sacrificed in the VO, CN and CO groups. Cyanide treatment and vascular occlusion was discontinued in the remaining $n = 6$ animals, each in the CN and VO treatments for the next 10 days (day 20). This represents the withdrawal phase and these groups were renamed CN-I and VO-I respectively. Author completed the IACUC training on Animal Use and a protocol number was already assigned to group (ABU13/Neu/008).

Cerebral blood vessels

The animals were anaesthetized using intraperitoneally administered sodium pentobarbital (50 IP). The root of the neck was dissected to expose the ascending aorta following which the brain was perfused with artificial cerebrospinal fluid [ACSF composition (mM): KCl, 2.5; MgSO₄, 1.0; NaH₂PO₄, 1.25; NaHCO₃, 26; d-glucose, 20; ascorbic acid, 0.45; CaCl₂, 2.0; and NaCl, 125 (osmolality, 290–310 mOsmol kg⁻¹; pH 7.3–7.4)] at 4°C. Subsequently, the tissues were perfused with freshly prepared formolcalcium and fixed thereafter in formolcalcium for 14 hours.

Tissue Preparation

The brain was dissected on a stereotaxic frame to obtain sagittal and corona sections of the MCA, periventricular zone (PVZ) and parietal cortex (PC) using specific coordinates [2.5 mm lateral to the median fissure (sagittal) and 1.5mm anterior to the bregma (corona section)]. Later, the sections were post-fixed in formolcalcium in a separate chamber (6 hours) and processed into paraffin wax embedded tissue blocks. Leica Bond RX (Leica GmbH, Germany) automated tissue stainer was used for immunohistochemical processing. All antibodies were procured from Novocastra (Leica Biosystems, Germany). Reagents and buffers used were molecular biology grade (99.9% pure) from Sigma-Aldrich (Germany).

Immunohistochemistry

7 μ m thick serial sections were prepared using a microtome (Leica) and were mounted on a glass slide in preparation for

antigen retrieval immunohistochemistry. Sections were immersed in urea overnight and transferred to a microwave for 45 minutes to expose the antigens and proteins. Primary treatment was done using bovine serum albumin (BSA) to block non-specific protein reaction in the tissue. Subsequent processing involved the use of specific biotinylated secondary antibodies (anti-CD31, anti-CD45 anti-NSE, anti-NF, anti-Ki-67 and anti-GFAP) diluted in PBS (a dilution of 1:200 was used for all secondary antibodies). The immunopositive reaction was developed using a polymer 3'3' Diaminobenzidine Tetrachloride (DAB; Sigma-Aldrich) with methenamine silver color intensification. The sections were counterstained in haematoxylin and treated with 1% acid alcohol (freshly prepared) to reduce the counter-stain intensity.

Cell Count and Analysis

The images were acquired using an Optronics Digital Camera connected to a computer interface (MagnaFire) and an Olympus BX-51 research microscope. The general structure of the pyramidal cells of the PC and round neurogenic cells of the PVZ were characterized using inter-reader variability. The total cell count was determined using a 10 × 10 grid graticulate at 400X magnification. For both the corona and sagittal sections, n = 2 fields were captured to obtain n = 4 fields per section. Subsequently, the average count for n = 4 fields was determined as the representative value.³³ Immunopositive cells in GFAP, NSE and Ki-67IHC were counted in Image J (NIH) and calculated using the method described in the previous paragraph. NF, CD31 and CD45 were expressed as intensity of IHC reaction products (+/-). The lumen and arterial wall of the MCA branch were measured using Open Office Draw Suite (Sun Microsystems) at a magnification of 100X. The data was plotted using a simple ANOVA (SPSS version 17.0; IBM) with significance set at $P < 0.05^*$, $P < 0.01^{**}$ and $P < 0.001^{***}$ for total and immunopositive cell counts.

Results

Histology of the MCA

The general morphology of the wall of the arteries was demonstrated in a corona section through the whole brain at approximately 1.3 mm anterior to the bregma. Increase in thickness of the wall of the arteries was characteristic of vascular occlusion (Figure 1-VO; 0.09 cm) and can be attributed in part to the mechanical stress induced by the cuffs for the treatment duration. The artery was also characterized by a narrower lumen (0.0028 cm), when compared with the control (0.036 cm) (Figure 1D). The effect of vascular occlusion in this group can be described anatomically as "induced vascular resistance" in the middle cerebral artery. The structural resistance observed in the global vascular occlusion treatment (VO) reduced after the withdrawal phase (VO-I). In the VO-I, the lumen/wall thickness ratio (LTR) increased significantly to 4.00 from the initial value (3.11) observed in the vascular occlusion treatment (Figure 1-VO-I). The increased LTR in this group corresponds to a reduction in wall thickness (0.008cm) and an increase in lumen width (0.032 cm; Figure 1D).

In cyanide treatment, a reduced LTR was seen (2.44) (Figure 1D); this was characterized by a prominent reduction in the lumen width (0.022 cm) and wall thickness (0.009cm) after the treatment phase (Figure 1-CN). In the withdrawal group for CN treatment, CN-I, the LTR value increased (3.00) when compared with

the control, indicating, a decreased resistance in the artery after the withdrawal. The increased LTR seen in CN-I was associated with an increase in the thickness of the tunica media (0.012 cm) and width of the lumen (0.036 cm) (Figure 1D).

CD31/CD45 (MCA)

CD31 and CD45 expression in the MCA (corona section) was determined to evaluate endothelial cell proliferation and the associated monocytic activity respectively. In VO (CD31⁺⁺) and CN (CD31⁺⁺⁺), the rate of endothelial cell proliferation increased (Figure 1; Table 1 and Figure 1D) when compared with the control after the treatment phase. This resulted in an increased intima-media layer thickness (CD31-endothelial activation) for CN and VO; although the expression of CD31 was higher in cyanide toxicity than vascular occlusion. However, after the withdrawal of cyanide treatment and vascular occlusion, a significant decrease in CD31-endothelial thickening was observed in the VO-I (CD31⁺) and CN-I (CD31⁻). Interestingly, we observed a decrease in monocytic-CD45 expression with an increase in endothelial-cell proliferation (\downarrow CD45/ \uparrow CD31) after the treatment phase (Figure 1; Table 1). The same association was observed after the withdrawal phase as CD45 increased (CD45⁺⁺⁺) with a corresponding decrease in CD31 expression (CD31⁺) in the VO-I (Figure 1B and C) (\uparrow CD45/ \downarrow CD31). In cyanide treatment, a similar *inverse relationship* was observed between CD31 and CD45.

Histology of the PC

The general morphology of the brain tissue was demonstrated by haematoxylin and eosin staining. Both CN and VO treatment groups showed degenerative changes in the parietal cortex (Figure 2A and Figure 2C) with a reduction in cell count per unit area (VO:16, CN:13) when compared to the control (24 cells per unit area) (Table 1; Figure 2F). Subsequently, an increase in cell count was observed after the withdrawal phase for both treatments such that CN-I recorded 16 and VO-I, 25 after this phase. In the VO-I, some cells showed features of resuscitation (Figure 2B) when compared with those of the CN-I (Figure 2C and 2D). Degenerative changes observed in the treatment groups include: vacuolated cytoplasm, loss of cellular projections, pale staining cell body, fragmented centrally placed nuclei and a diminished nucleoplasm.

Histology of the PVZ

Prominent cellular changes occurred in the PVZ of both models of ischemia after the treatment duration. The degenerative changes observed in the cells of the PVZ are similar to those of the cortical cells described above. It is important to note that the cells of PVZ often lack cellular projections; thus the adopted criteria for identifying degenerating cells in the PVZ excludes loss of cellular projections. The CN treatment group showed significant cell loss in the PVZ¹³ when compared with the control.²⁴ The cell count increased in the withdrawal group for cyanide treatment (CN-I; 15) but was less than that seen in the control. Vascular occlusion (VO) induced minor degenerative changes in the PVZ with minimal cell loss¹⁶ after the treatment phase. However, in the vascular occlusion treatment, no significant change in cell count was observed after the withdrawal phase (Table 1; Figure 2F). Generally, the distribution of degenerating neurogenic cells in vascular occlusion (Figure 2A) and cyanide treatment (Figure 2C) groups demonstrates the role of ischemia in induced degeneration in the plastic (PVZ)

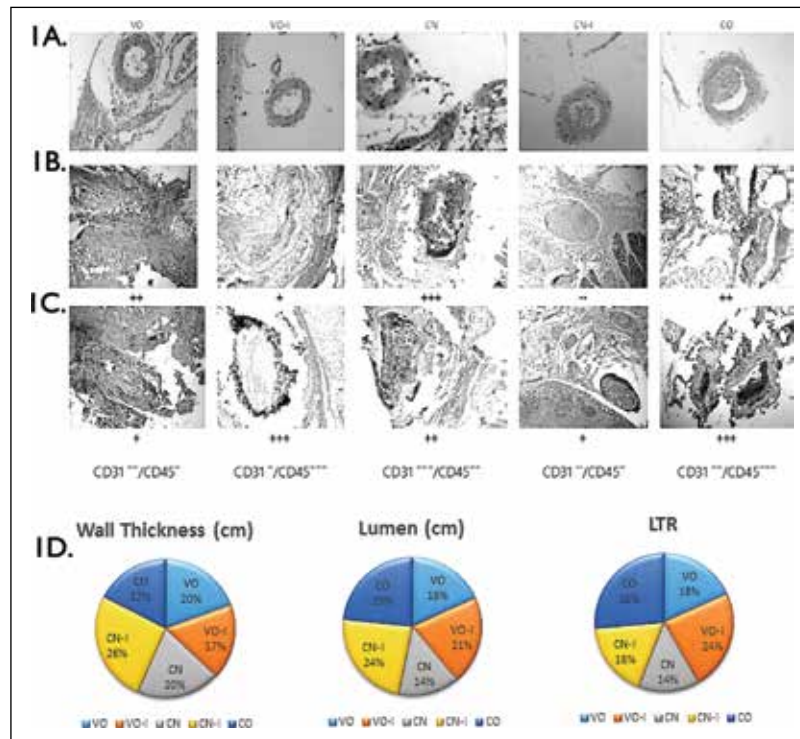


Fig. 1: Coronal section of the brain showing a branch of the MCA close to the third ventricle (A) Microscopic anatomy of the artery demonstrated in haematoxylin and eosin staining (Magnification X100) to show the lumen and tunica media/intima in cyanide toxicity and vascular occlusion; after the treatment and withdrawal phases. An increase in the tunica media/intima thickness was observed in VO and was accompanied by a decrease in lumen width. In cyanide toxicity, degenerative changes were observed in the tunica media/intima; consequently, a decrease in wall thickness and lumen width was recorded in this group. A common set of event in the CN and VO is the decrease in lumen width and an increase in vascular resistance shown by the lumen width/wall thickness ratio (Figure 1D). After the withdrawal phase, regenerative changes such as increased lumen width, reduced vascular resistance and increased cell count were seen in the CN-I and VO-I. Degenerative changes were more pronounced in cyanide toxicity after the treatment phase with a LTR value of 2.44. Sequel After to the withdrawal of cyanide treatment in CN-I, the LTR value increased to 3.67 after the withdrawal phase, thus, a decreased vascular resistance (Figure 1D). Similarly, after vascular occlusion, vascular resistance increased in the artery (3.11) when compared with the control (4.55) and decreased after the withdrawal phase (VO-I; 4.00). This further supports the change in lumen width observed in histology after the treatment (↓lumen width and ↓LTR) and the improvement seen after the withdrawal phase (↑lumen width and ↑LTR). (B) CD31 immunohistochemistry to demonstrate endothelial adhesion molecule PECAM-1 during endothelial proliferation in cyanide toxicity and vascular occlusion induced oxidative stress. Endothelial proliferation (↑CD31) was observed in cyanide toxicity (CD31⁺⁺⁺) and vascular occlusion (CD31⁺⁺) after the treatment phase. Similar to our observations in the LTR and histology (Figure 1A and 1D), a reduction in endothelial proliferation (↓wall thickness) was observed after the withdrawal phase. This was highly significant in CN-I (CD31⁻) and was less significant in VO-I (CD31⁺) (C) Blood monocytes and phagocytes (CD45) were demonstrated around the artery to determine their role in pro-inflammation (treatment) and remodeling (withdrawal) during oxidative stress. Interestingly, VO (CD45⁺) and CN (CD45⁺⁺) showed a significant reduction in monocyte expression when compared with the control (CD45⁺⁺⁺) signifying the non-involvement of these cells in pro-inflammatory response. However, after the withdrawal phase, the expression of CD45/monocytes increased significantly in VO-I (CD45⁺⁺⁺) and no significant change was observed in CN-I (CD45⁺). Subsequent analysis reveals that CD45/monocyte expression was associated with post-ischemia remodeling and not inflammatory response in oxidative stress. Furthermore, the magnitude of vascular remodeling was more significant in vascular occlusion than cyanide toxicity (D) Pie chart representation of the wall thickness, the lumen width and the LTR.

Table 1: Cell counts in the PC and PVZ. The count represents the average of cell distribution in the sagittal and corona sections. The NF, CD31 and CD45 were assigned +/- or + based on the intensity of immunoreaction colour deposits

Brain	VO	VO-I	CN	CN-I	Control
PVZ					
Total Cell Count	16	25	13	15	17
GFAP	21	18	13	16	24
NSE	14	11	5	29	14
Ki-67	10	5	8	6	6
PC					
Total Cell Count	16	15	13	16	24
GFAP	23	27	35	17	15
NSE	3	4	2	8	10
Ki-67	5	9	5	4	8
NF	++	++++	+/-	+	+++
Blood Vessel					
CD31	++	+	+++	--	++
CD45	+	+++	++	+	+++

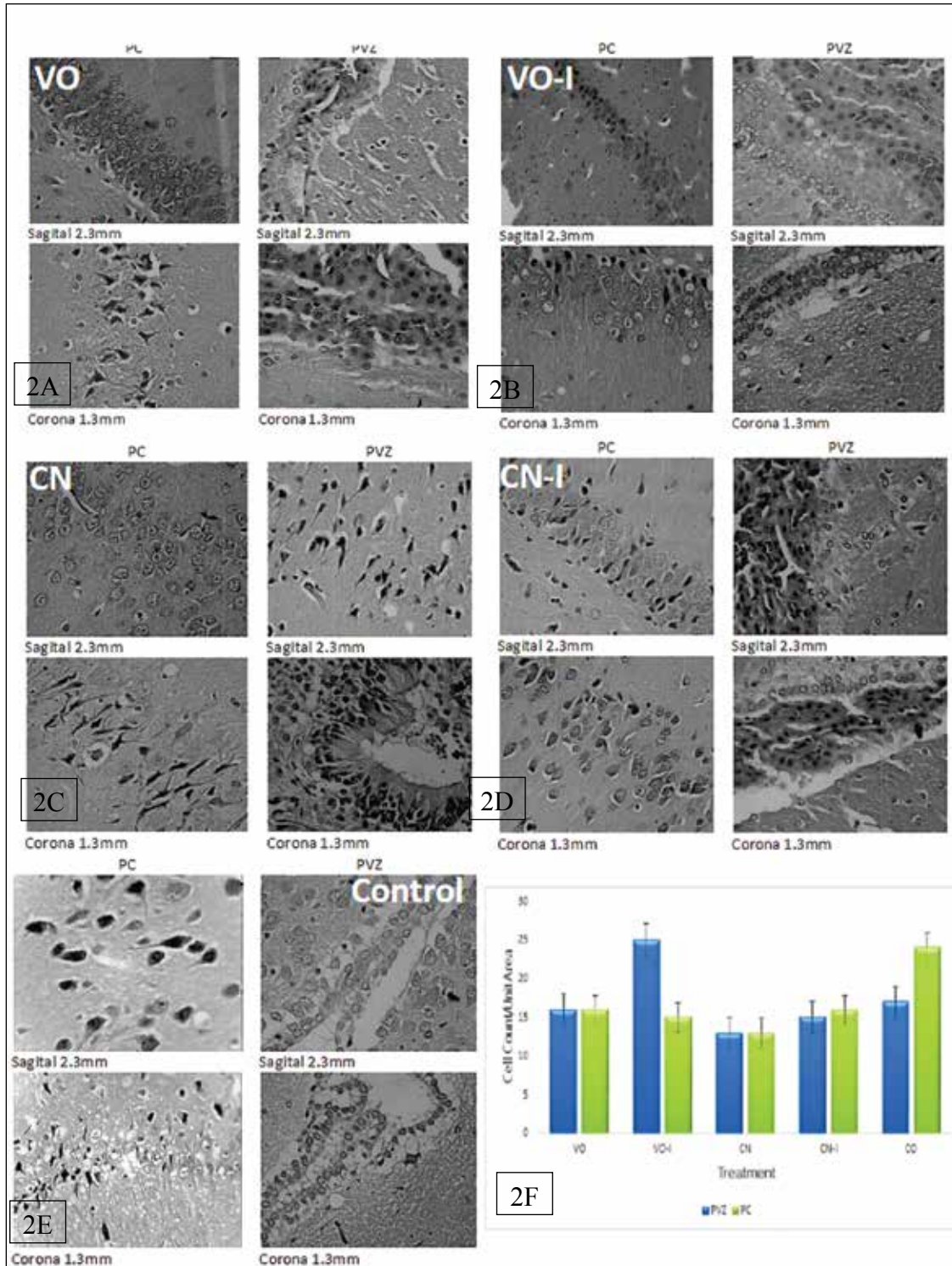


Fig. 2: General morphology of the PC and PVZ for the treatment groups and the control (A) Degenerative changes are characteristic of vascular occlusion both in the PC and PVZ as the cell count reduced when compared to the control (B) In the withdrawal group for vascular occlusion; VO-I, the degeneration reduced and cell proliferation increased in the PVZ. Also, cell count and cell morphology gave scores similar to those of the control (Table 1) (C) Cyanide treatment induced aggressive degenerative changes ranging from reduced cell number, loss of cellular projections, pale staining cell bodies and vacuolar spaces around the neurons of the PC and PVZ (D) An improvement in cell count and structure (PC and PVZ) was observed in the CN-I following the withdrawal of cyanide treatment. Cell count increased in the PVZ of the CN-I, similar to what was observed in VO-I, but was less significant when compared versus the control and VO-I (E) Control; the structure of the PVZ is well defined with rounded cells organized into layers beside the highly vascularised third ventricle. The neurons of the PC are characterized by prominent neuronal projection, dark staining cell body and cell count was higher than those of the treatments (Magnification X400). (F) Bar chart representation of the total cell count in the PC and PVZ (Mean±SEM).

and non-plastic (PC) brain areas. Interestingly, the results suggest a differential rate of degeneration for these brain areas. Specifically, we observed a higher cell loss in the PC than the PVZ for the same threshold of assaultin cyanide toxicity and vascular occlusion.

GFAP PC

We next investigated the distribution of glia cells in the PC and PVZ after the treatment and withdrawal phases using specific antibody interaction to show the expression of type III intermediate filament (GFAP) in astrocytes. Similar to our previous findings,²⁵ we observed a variation in glia count for the PC and PVZ in cyanide treatment. In addition, this study has shown a similar trend exists for the PC and PVZ after vascular occlusion.

A significant increase in glia count was observed in the PC post cyanide treatment (35; Figure 3C and 3F) when compared with vascular occlusion (23; Figure 3A). From these results, it is evident that degeneration progressed faster in CN treatment than in VO, hence, the higher glia count in CN treatment after the treatment phase (Figure 3F; Table 1). In the withdrawal groups, glia activation was higher in the VO-I (27; Figure 3B) and lower in the CN-I (17; Figure 3D) when compared with the control. This suggests that in cyanide treatment degeneration proceeded faster during the treatment period and receded upon withdrawal - while the opposite occurred in case in vascular occlusion.

GFAP PVZ

The glia count decreased significantly in the PVZ after vascular occlusion was induced (21; Figure 3A) when compared with the control (24; Figure 3E). After the withdrawal phase, a further decrease in glia count was observed in the VO-I (Figure 3B-PVZ) having a score of 18 (Figure 3B). In the CN treatment, glia count increased significantly (30; Figure 3C) after the treatment phase but decreased slightly in the withdrawal phase (25; Figure 3D).

NSE PC

The importance of neuronal metabolism in determining the significance of glia activation and other cellular changes associated with cyanide toxicity and vascular occlusion is important. Neuron specific enolase (NSE), a gamma enolase, expressed in immature neurons, early in neurogenesis, and adult neurons in oxidative stress was labelled in the PC to demonstrate neuron specific oxidative stress, and to distinguish neurons from glia cells. We observed a decrease in NSE immunopositive cell count after the treatment phase [VO (3; Figure 4A) and CN (2; Figure 4C)] and an increase after the withdrawal phase (Figure 4B; Table 1). The most significant change in NSE expression was observed in the cyanide treatment group, such that the withdrawal (CN-I; 8) recorded NSE scores four times the treatment (CN; 2) (Figure 4C, 4D and 4F). All the treatments and withdrawal groups recorded NSE scores significantly lower than the control value (10; Figure 4 E).

NSE PVZ

In the neurogenic zone, the least NSE score was recorded in the CN treatment (Figure 4C). (However, withdrawal of cyanide treatment caused a significant increase in NSE count; from 14 in CN to 29 in CN-I (Figure 4F). This supports the previous findings that CN triggers a more rapid degeneration that reverses after withdrawal). Interestingly, in vascular occlusion, the NSE score

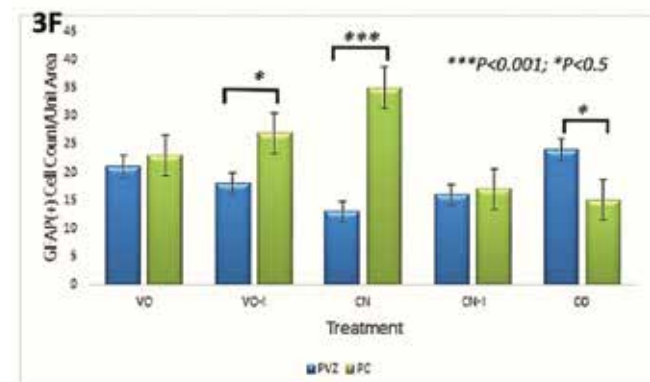
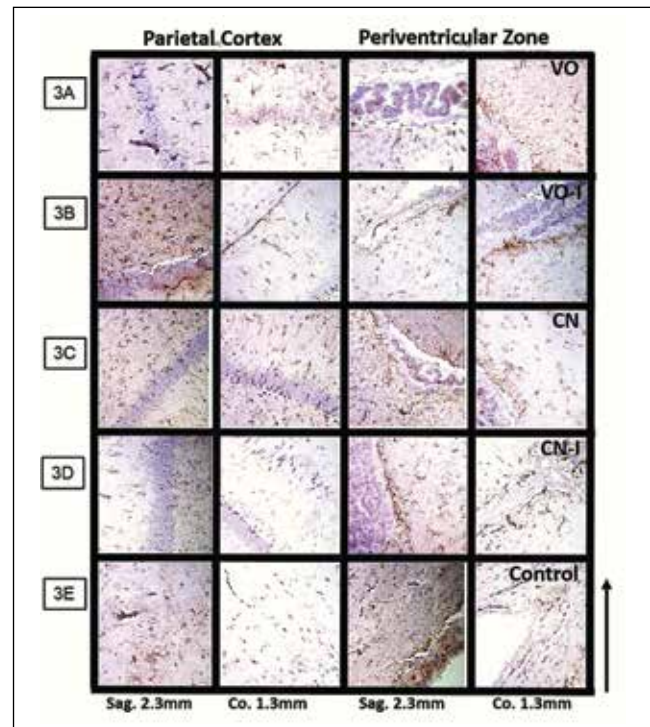


Fig. 3: Distribution of GFAP in the PC and PVZ (A) mapping of astrocytes via IHC staining with anti-GFAP in the PC and PVZ of rats subjected to vascular occlusion. Increased immunoreaction depicts ependymal astrocyte proliferation around the blood vessels rich PVZ and glia activation in the parietal cortex (B) after the withdrawal phase, a reduction in astrocyte (GFAP) count was observed in the PVZ but increased in the PC ($P < 0.05$) when compared with the control (C) The most significant glia activation was observed after cyanide toxicity with a glia count of 35 in the PC (significant at $P < 0.001$ when compared with the control) (D) after the withdrawal phase, glia activation reduced in the PC and increased in the PVZ of cyanide treatment group (CN-I) (E) The control distribution of glia cells in the PC and PVZ (Magnification X100). (F) Bar chart representing the immunopositive glia cell counts in the PC and PVZ (Mean \pm SEM).

was higher in the treatment (14; Figure 4A and Figure 4F) and decreases after withdrawal (Figure 4B and Figure 4F).

Ki-67 PC

This is a cytoplasmic inclusion found in dividing mammalian cells, including neurons in early neurogenesis. Ki-67 was demonstrated to determine the probable event of cell prolifera-

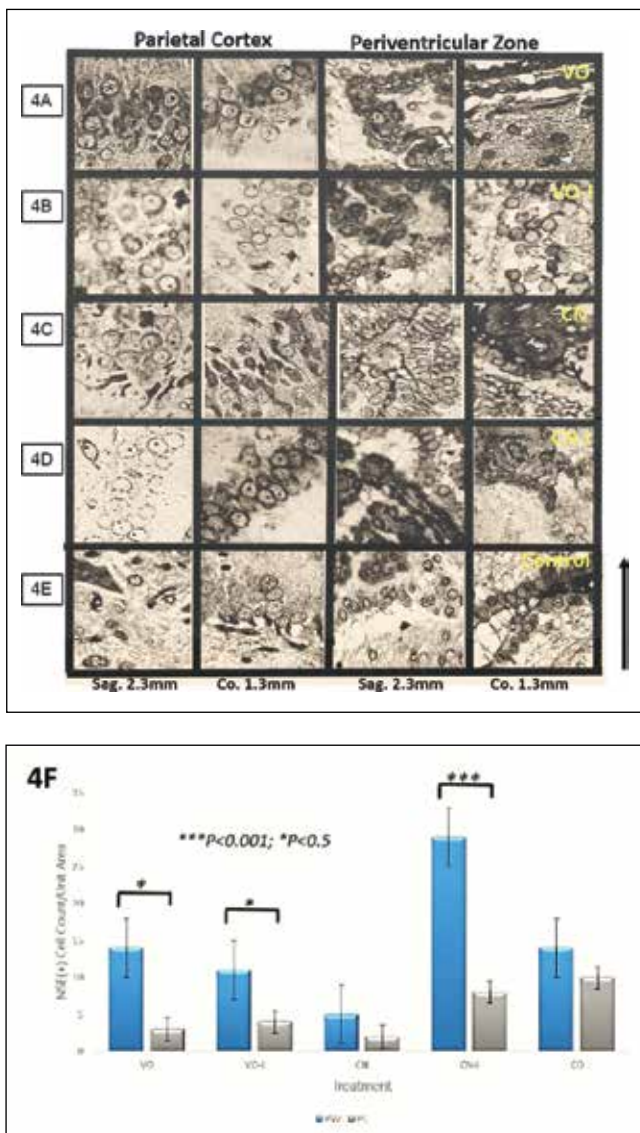


Fig. 4: Distribution of NSE in the PC and PVZ. The γ -enolase was shown in IHC using anti rat-NSE to demonstrate the metabolic switch from α -enolase in oxidative stress or neurogenesis in the PC and PVZ (A) a reduction in NSE (+) cell count was observed after the treatment phase in vascular occlusion ($P<0.001$) when compared with the control (B) surprisingly, the withdrawal group of vascular occlusion (VO-I) showed no significant change in NSE (+) cell count in the PVZ and recorded a reduction in NSE (+) in the PC ($P<0.05$) versus the control (D) Cyanide treatment withdrawal group showed a good yield in NSE (+) cell count both in the PC (8) and the PVZ (29) ($P<0.001$) when compared with VO/VO-I (E) Control group PVZ and PC showing the distribution of NSE positive cells in the molecular layer of the PC and the outer border of the PVZ (Magnification X400) (F) Bar chart representing the score for anti-NSE positive cell distribution in the PC and PVZ (Mean \pm SEM).

tion in the PC and (or) PVZ in the two models of ischemia. Cell proliferation was lower in the non-plastic PC when compared to the neurogenic PVZ. In vascular occlusion, Ki-67 immunopositive cell count recorded a score of 5 (Figure 5A and Figure 5H); the appearance of these cells suggests they might be glia rather than neuronal. The rate of proliferation increased in the withdrawal for this category having a score of 9 in VO-I

(Figure 5B), similar to the trend observed in GFAP distribution. However, in cyanide toxicity, withdrawal had little effect on cell proliferation in this region increasing from 4 in CN (Figure 5C) to 5 in CN-I (Figure 5D and 5H). Cell proliferation was lower in CN and CN-I when compared with vascular occlusion and the control (Figure 5E and Figure 5H).

Ki-67 PVZ

Subsequent analysis of Ki-67 immunopositive cells showed a score of 10 in VO (10; Figure 5A) and 8 in CN (8; Figure 5C). These values were higher than those recorded in the withdrawal groups, that is CN-I (6; Figure 5D) and VO-I (5; Figure 5B). The results suggest that oxidative stress drives proliferation in the neurogenic PVZ. Severally dividing and migrating neurons *in vivo* stained positive in Ki-67as shown in Figure 5F and 5G.

Neurofilament

The immunoreactivity of NF demonstrates the extent of neuronal process degeneration in the models of ischemia. Because the PVZ is void of cellular projections, NF was demonstrated only in the PC. The least NF deposition was found in cyanide treatment. This further supports the earlier findings in GFAP and NSE count which show that CN caused a more rapid degeneration than VO for the treatment duration. Also, regenerative changes occurred faster in vascular occlusion withdrawal group (VO-I: NF⁺⁺⁺⁺) as compared to the initial treatment (VO) group (NF⁺⁺). In cyanide toxicity, degeneration of neurofilament was observed (NF^{+/+} in the CN) mostly in the fibrous layers of the cortex. These degenerative changes were reduced in the withdrawal group (CN-I), having a significant increase in deposition of neurofilament (NF⁺⁺) when compared with the control (Figure 6; Table 1).

Discussion

Taken together, the results of this study have shown that endothelial alteration accompanies neuron/glia change in vascular occlusion and cyanide toxicity. The observed morphological alteration involved an increase in endothelial activation (CD31) accompanied by a reduction in monocytic expression (CD45) after the treatment phase. Interestingly, this was reversed in the withdrawal phase as endothelial activation reduced and monocytic expression increased. We have also shown that the magnitude of endothelial proliferation determines the extent of PC/PVZ degeneration or PVZ proliferation in chemotoxicity and vascular occlusion. Ultimately, we attributed these changes to glia activation (\uparrow GFAP), coupled with an increased neuronal metabolic demand (\downarrow NSE) in the cortex and PVZ. Although the observed change in neuron/glia metabolism and microvasculature of the brain during oxidative stress is believed to be a homeostatic response to balance oxygen supply and metabolism, however, certain differences were observed in the stress response generated in vascular occlusion, cyanide toxicity and the corresponding withdrawal groups.

Vascular Occlusion

Vascular occlusion induced proliferative changes in the blood vessels, and degeneration in the PVZ and PC post treatment (Figure 1D). Subsequently, this was reversed after the withdrawal period as the cell count increased in the PC, endothelial proliferation reduced (CD31⁺) and monocytic expression increased (CD45⁺⁺⁺) (Figure 1B and Figure 1C). The observed changes were regarded as an inverse link between neurogenesis

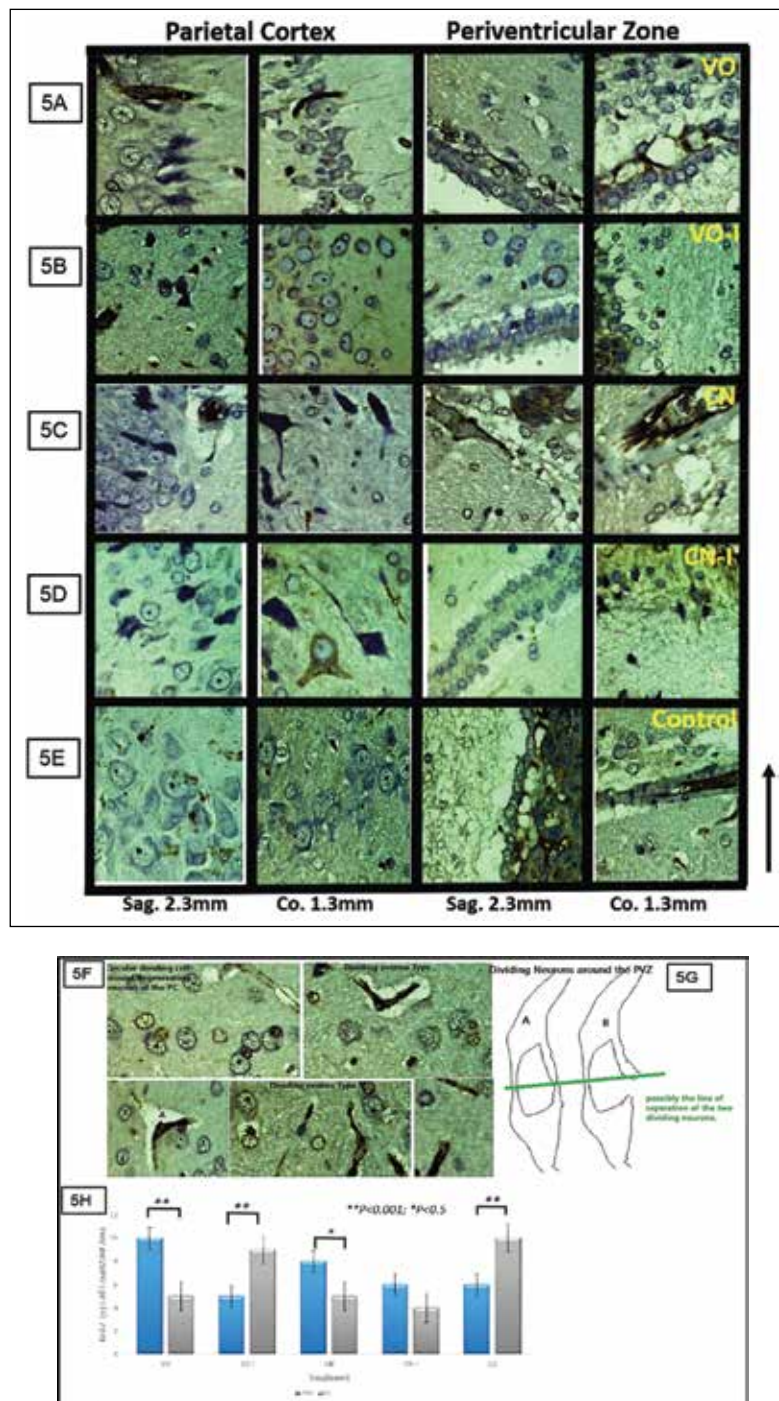


Fig. 5: A-E. IHC Demonstration of Ki-67 cytoplasmic inclusions in the PC and PVZ. (A) Cell proliferation was higher in the PVZ compared to the PC in VO after the treatment phase **(B)** After the withdrawal phase, increased cell proliferation was observed in the PC than in the PVZ of the VO-I treatment when compared with the VO and control ($P < 0.01$). However, the proliferating cells were glia (\uparrow GFAP) rather than neuronal (NSE) **(C)** CN treatment caused a reduction in cell proliferation in the PC (\downarrow Ki-67) when compared with the control. However, an increase in cell proliferation was observed in the PVZ (\uparrow Ki-67) when compared with the control. This suggests that oxidative stress also drives cell proliferation in certain cells of the PVZ despite the cell loss observed in total cell count. Further analysis reveals astrocytic proliferation was more significant (\uparrow GFAP) than neuronal proliferation (NSE) in the PVZ ($P < 0.05$). **(D)** Following the withdrawal of cyanide treatment, the rate of cell proliferation changed only slightly in the PC but significantly reduced in the PVZ of the CN-I group ($P < 0.05$). In furtherance, the decrease in Ki-67 corresponds to a decrease in astrocyte (\downarrow GFAP) and monocyte (\downarrow CD45) count after the withdrawal phase in this group **(E)** demonstration of Ki-67 positive cells in PC and PVZ of the control group. **5F-H Pattern of cell division in the PVZ (F)** several dividing neurons (stained positive to anti-Ki-67) showing polarity (or cytokinesis *in vivo*). The shape of these cells is unique and often has midline ring and 2 limbs adjoining these separating cells. Furthermore, our previous results (Ogundele et al., 2014) show that these cells are neuronal as they stained positive to NSE in IHC (Magnification X400). **(G)** The dividing cells are further illustrated using line graphics **(H)** Bar chart representing immunopositive cell count in Ki-67 IHC of the PC and PVZ (Mean \pm SEM).

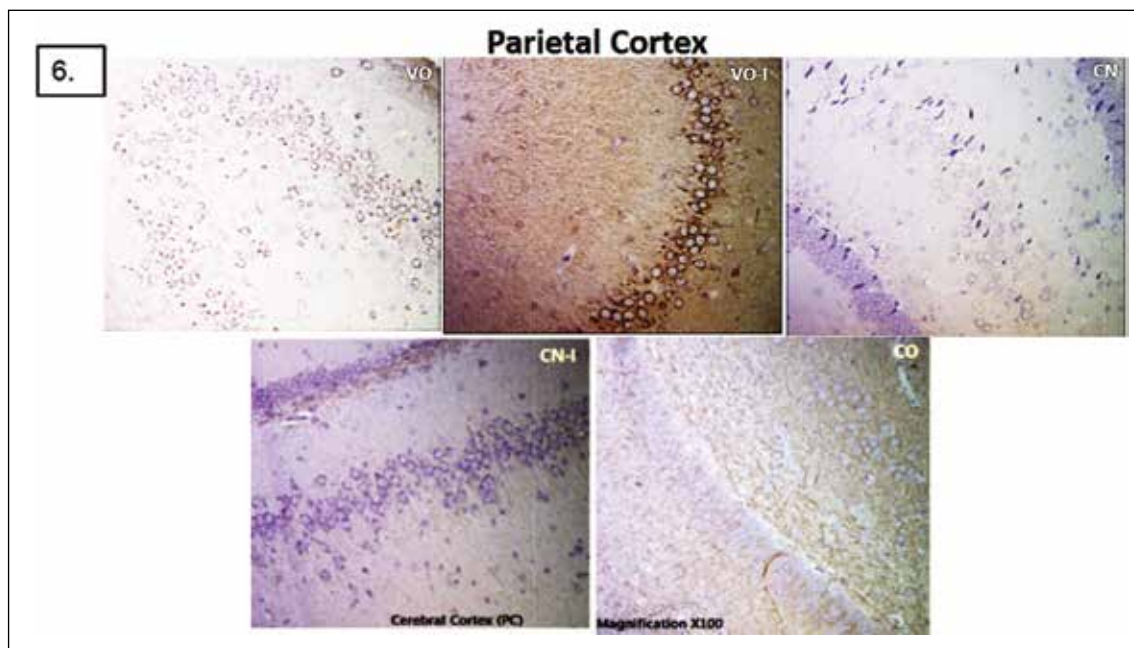


Fig. 6: Neurofilament distribution and lamellation in the parietal cortex (A) Loss of NF immunodeposition in VO (NF⁺⁺) indicates degeneration in the PC after the treatment phase when compared with the control (NF⁺⁺⁺) (B) In the withdrawal group for vascular occlusion (VO-I), deposition of NF (NF⁺⁺⁺⁺) was observed in the PC around the neurons of the pyramidal cell layer. This indicates re-modelling of neuronal projections in this region after the ischemic injury (C) Cyanide toxicity induced degenerative changes characterized by heavy loss of neurofilament in the cortex (NF^{+/+}) when compared with the control (NF⁺⁺⁺). (D) Similarly, an increase in NF was observed after the withdrawal phase (CN-I; NF⁺) but was less significant when compared with VO-I (E) distribution of neurofilament in the PC of the control. This shows a well-defined cellular and fibrous layer with filaments extending from one layer of the cortex to the next (Magnification X100).

and angiogenesis modulated through signaling pathways involving angiogenic cells and immature neurons in remodeling post-ischemia.^{34–36} We next examined the distribution of Ki-67 and NSE immunopositive cells in the PC and PVZ and observed active cell migration and metabolism in the PC and PVZ after the withdrawal phase. This is supported by the findings of Rossell et al. (2013) where endothelial progenitors were used as stimulants for angio-neurogenesis post ischemia induced by MCA occlusion.³⁷ In order to confirm neuronal cell proliferation, first we analyzed the distribution of neuron progenitors (NSE/Ki-67) in the PVZ and found that they were localized in the upper 2 or 3 layers of the PVZ. Subsequent analysis of the NSE/Ki-67 progenitor cells show that further away from the PVZ, they assume a spindle shape and become polarized (Figure 5F and 5G). In addition, they separate along the midline with two (2) cellular processes adjoining the two daughter cells (Figure 5G) with the upper cell extending towards the subcortical area and the lower cell directed towards the upper cell layer of the PVZ (Figure 5F). Interestingly, our previous study described such pattern of cell separation in neurogenesis using NSE immunolabeling to show proliferation in cells of the PVZ *in vivo*. It was observed that dividing neurogenic cells were characterized by two crus (limbs) around the separation ring and were oriented in opposite directions.²⁵ Since the neurogenic progenitor cells can divide to yield neuron and glia, we next distinguished gliogenesis from neurogenesis using the proposition by Robertson (2014).³⁸ This involved statistical comparison of the GFAP/NSE count in the PC and PVZ, followed by a direct correlation with the Ki-67 count. We observed an increase in cortical Ki-67, most of which were restricted to the subcortical areas and

mostly coincided with the location of glia cells (GFAP) rather than neuron (NSE) (Table 2).

In addition to neurogenic cell division, histology of the PVZ revealed a stratified arrangement of cells having 4–6 layers of rounded cells. Further characterization in IHC showed that the glia-progenitor cells (GFAP⁺) were closer to the blood vessels (lower 3 layers around the third ventricle) while the NSE positive cells (neuron progenitor) were sparsely located in the upper 2–3 layers close to the lower limit of the cortex (Figure 4E and 2E). We also observed an increased glia count around the blood vessels and degenerating cortical neurons. This was attributed to rapid re-modelling of the BBB and a signal of neuronal metabolic support/degeneration in the cortex. Consequently, repair was observed after the withdrawal phase as shown in the increased neurofilament (NF) deposition from NF⁺⁺ in the VO to NF⁺⁺⁺⁺ in VO-I.

Chemotoxicity

In cyanide toxicity, the observed degenerative changes were widespread and severe when compared with the control and the vascular occlusion group. However, after the withdrawal phase, an increase in cell count was recorded in the PC and PVZ (Figure 2C and 2D). Endothelial activation was more significant in cyanide treatment (CD31⁺⁺⁺) and was accompanied by a reduction in monocytic expression (CD45⁺⁺). A difference in angiogenic expression was observed for cyanide toxicity when compared with the vascular occlusion treatment as degeneration was seen in the tunica media of the MCA for CN, and proliferation was seen in VO (Figure 1). In cyanide

Table 2: GFAP/NSE ratio for the treatments and control group. The GFAP/NSE ratio shows rate of glia activation compared with degeneration in the PVZ and PC

PC					
	VO	VO-I	CN	CN-I	CO
GFAP	23	27	35	17	15
NSE	3	4	2	8	10
GRAP/NSE	7.67	6.75	17.5	2.13	1.5
PVZ					
GFAP	21	18	30	25	18
NSE	14	11	5	29	14
GRAP/NSE	1.5	1.64	6.0	0.86	1.28

toxicity, the expression of CD31⁺⁺⁺/CD45⁺⁺ show that the endothelial proliferation was rapid due to ROS and NO mediated pathways as previously described.³⁹ In the withdrawal group, a shift in angiogenic expression was observed such that endothelial proliferation was negative and monocytic activity also declined (CD31⁻/CD45⁺). The expression of CD31⁻/CD45⁺ in the CN-I indicates that endothelial proliferation and vasculogenesis occurred minimally post withdrawal; similarly, a low Ki-67 count was associated after cyanide withdrawal (Figure 4C, 4D, 5C and 5D).

Glia activation was highest in cyanide treatment showing the more aggressive nature of this form of ischemia with a score of 35 in the PC and 30 in the PVZ. This was also accompanied by a reduction in neuron count; with the most significant loss in the PC. However, a reduction in glia count was seen after the withdrawal phase with a corresponding increase in NSE count. A major evidence of neuronal survival was seen in neurofilament deposition in the cortex, which increased significantly after the withdrawal phase (NF⁺⁺⁺⁺) (Figure 6).

Endothelial activation is characterized by an increase in CD31 expression in induced oxidative stress. This is accompanied by a reduction in monocyte count (↓CD45) and an increase in glia count (↑GFAP). Both VO and CN induced these set of changes, although the extent of endothelial-glia activation was more significant in CN treatment. The magnitude of the endothelial activation also corresponded with the observed neuronal degeneration, being more significant in cyanide treatment. After the withdrawal phase, a decrease in endothelial activation facilitated cell proliferation in the PVZ, thus suggesting an inverse relationship between neurogenesis and angiogenesis in stress. Ki-67/GFAP and Ki-67/NSE distribution suggests the proliferation was glial rather than neuronal. However, certain neurogenic cells divided after the induced stress (Figure 5F and 5G) while expressing NSE in the upper 2–3 layers of the PVZ. The observed degenerative changes were reversed after the withdrawal phase for cyanide toxicity and vascular occlusion.

Angiogenesis in Ischemia

Previous studies have shown that inflammatory bacterial infection, chemotoxins, stroke/plaques, drug abuse can cause injuries to the unit arrangement at micro-vessel level (environment) of the brain.^{38,40} A major cell type around the neurovascular structures is the CD45⁺-Monocyte (phagocytes) which is activated in neurodegeneration and inflammation to remove degenerating neurons and participate in remodeling of the blood vessels. The increase in the expression of these cells (CD45+)

demonstrates the activity of phagocytes in re-conditioning during oxidative stress, a similar role performed by microglia in stress.^{41,42} Our results revealed that ischemia induced pro-inflammatory events which involved glia activation, increased in endothelial proliferation and decreased monocyte count. Furthermore, we observed a decrease in glia activation (↓GFAP) and endothelial proliferation (CD31) sequel to the withdrawal of the ischemic assault with a corresponding increase in monocyte count. Consequently, it suggests the role of CD45 monocytes in the recovery and remodeling of the neurovasculature rather than being a pro-inflammatory mediator; similar to the findings of Brambilla et al. (2014).⁴¹

Astrocytic activation and NSE in stress

The relationship between the neuron (NSE) and astrocytes (GFAP) is deeply rooted in function, metabolism and structure. The expression level of GFAP and NSE has proven to be of clinical significance, especially in diagnosis of degenerative diseases and progression of traumatic brain injury.⁴³ The level of these proteins are usually elevated by several folds in the cerebrospinal fluid and blood of neurosurvival patients (NSE/S100b by 18.3 folds and GFAP by 4.6 folds).^{43,44} This suggests that GFAP/NSE profile can add to the clinical assessment of the primary damage and predicting the outcome after some chemotoxicity or vascular occlusion.

Ischemic injury causes cellular activation and degeneration which often leads to the release of cell-type-specific proteins.^{43–45} The GFAP/NSE profile is a reflection of cellular and sub-cellular events and differences between neuron and astrocytes under these conditions.⁴⁶ Although NSE is expressed in neurogenesis and stress, our results suggest that NSE levels in neurogenesis are higher than that observed in stress, similar to the findings of Amorino and Parsons, (2004).⁴⁷ Comparing the two models of ischemia, NSE level was higher in VO than CN, thus indicating the role of decreased endothelial cell proliferation (CD31) and angiogenesis in speeding up NSE activation (See also Table 1). The most predominant cell proliferation in the PC was astrocytic as seen by the GFAP/NSE ratio (Table 2). This trend also shows that oxidative stress reduced NSE in cortical degeneration and increased glia presence in these degenerating brain regions. Comparing the GFAP/NSE ratios, in the VO and CN showed that glia activation was higher than NSE expression in both treatment groups (CN-17.5 and VO-7.67). A higher GFAP/NSE ratio in the CN treatment indicates a more rapid progression of ischemic assault when compared with VO and the control (with an index of 1.5). In addition, this index

showed that glia activation was more active in the PC than the PVZ. In the withdrawal groups, VO-I scored 6.75 in the PC and 1.64 in the PVZ while CN-I scored 2.13 in the PC and 0.86 in the PVZ; this confirms reduction of glia activation and an increase in neuronal survival (NSE) in these groups. Other studies used a similar comparison in CSF assays as a predictor of progression of degeneration in traumatic brain injury patients.^{43,48}

Conclusion

Cyanide toxicity and vascular occlusion can be described through the bidirectional model of the endothelium-neuralendothelium-neural tissue interphase (BBB). From these findings we hypothesise that cyanide toxicity induced the outward signal (neurodegeneration to vascular changes) while vascular occlusion causes endothelial proliferation which precedes neurodegeneration (inward signal).

Vascular occlusion induced neuronal degeneration after endothelial and glia activation caused by the mechanical stress and hypoxia. The endothelial activation was seen as an increased vascular resistance, probably associated with increased endothelial nitric oxide which is associated with neuronal oxidative stress and degeneration after the treatment phase.

Cyanide diffused through the membrane to inhibit cytochrome C oxidase (CcOX) in the mitochondria. As a result, ROS and NO are released, signalling neuronal oxidative stress and glia activation. The interaction between ependymal glia and endothelial cell is important in the associated endothelial activation which occur after onset neurodegeneration and glia activation.

We conclude that cyanide toxicity and vascular occlusion induced oxidative stress and neurodegeneration in the brain (\downarrow NSE). This was associated with endothelial proliferation (\uparrow CD31) and glia activation (\uparrow GFAP) after the treatment phase, thus signifying degenerative and pro-inflammatory changes. However, the significance of degeneration was pronounced in cyanide treatment when compared with vascular occlusion. Subsequently, withdrawal of cyanide treatment and vascular occlusion induced a reduction in endothelial proliferation (\downarrow CD31) and glia activation (\downarrow GFAP). In addition, an increase in neuron count (\uparrow NSE) and monocytic activity (\uparrow CD45) was observed which is an indication of neurosurvival and vascular remodeling after this phase. Similarly, we recorded an increase in cell proliferation (\uparrow Ki-67) and neurofilament deposition (\uparrow NF) after the withdrawal phase. Degenerative changes were more significant in the PC than PVZ; also, PVZ showed an increase in cell proliferation after the withdrawal phase. Finally, cyanide toxicity improved better than the vascular occlusion after the withdrawal period.

Abbreviations

NSE (neuron specific enolase; γ enolase), GFAP (glia fibrillary acidic protein; a type III intermediate filament), Ki-67 (cell proliferation marker), NF (neurofilament), CD31 (PECAM-1; an endothelial adhesion molecule), H&E (haematoxylin and eosin), CD45 (blood monocyte/phagocyte marker), LTR (lumen width/wall thickness ratio), PC (parietal cortex), PVZ (periventricular zone), VO (vascular occlusion), VO-I (vascular occlusion withdrawal), CN (cyanide toxicity), CN-I (cyanide toxicity withdrawal), BBB (blood brain barrier).

Acknowledgement

We acknowledge the contributions of the Anatomy technicians in maintaining and caring for the animals throughout the peri-

od of the study. Our sincere appreciation to Prof. Kirk Deitsch of the Weill Medical College of Cornell University, New York, USA, for giving us access to the Olympus BX 51 research Microscope and Optronics Camera for the image acquisition and analysis.

Funding

This work is supported by the ISN-CAEN 1B of August, 2013 issued by the International Society for Neurochemistry. Also, the Disease Model Mechanism Travelling Fellowship Grant TF476 issued by the Company of Biologists LTD, Cambridge UK. Both grants are awarded to OOM.

Author Contribution

Ogundele O Michael: Initiated and designed the study, **Balogun W Gbolahan, Ansa E Cobham, Amin Abdulbasitand, Ishola Olakunle:** All contributed in the implementation of the research, analysis of results and report writing.

This article complies with International Committee of Medical Journal editor's uniform requirements for manuscript.

Conflict of Interest: (COI) Statement: The Authors hereby declare there is no conflict of interest associated with this study or any of the procedures and materials used for the purpose of the study.

Received Date : 8 October 2014; Revised Date : 6 January 2015;

Accepted Date : 6 February 2015

References

1. Goodin DS, Ebers GC, Cutter G, et al. Cause of death in MS: long-term follow-up of a randomised cohort, 21 years after the start of the pivotal IFN β -1b study. *BMJ Open*. 2012; 2(6).
2. Pham JC, Huang DT, McGeorge FT, et al. Clarification of cyanide's effect on oxygen transport characteristics in a canine model. *Emerg Med J*. 2007; 24(3): 152–6.
3. Shen Q, Du F, Huang S, et al. Neuroprotective efficacy of methylene blue in ischemic stroke: an MRI study. *PLoS One*. 2013; 8(11): e79833.
4. An C, Shi Y, Li P, et al. Molecular dialogs between the ischemic brain and the peripheral immune system: Dualistic roles in injury and repair. *Prog Neurobiol*. 2014; 115 6–24.
5. Ishikawa H, Tajiri N, Shinozuka K, et al. Vasculogenesis in experimental stroke after human cerebral endothelial cell transplantation. *Stroke*. 2013; 44 (12): 3473–81.
6. Chaitanya GV, Cromer WE, Parker CP, et al. A recombinant inhibitory isoform of vascular endothelial growth factor164/165 aggravates ischemic brain damage in a mouse model of focal cerebral ischemia. *Am J Pathol*. 2013; 183(3): 1010–24.
7. Oudemans EA, Frijns CJ, Klijn CJ. Multiple cerebral infarctions and intracranial vessel abnormalities. *JAMA*. 2013; 310(24): 2668–9.
8. Jackman K, Iadecola C. Neurovascular Regulation in the Ischemic Brain. *Antioxid Redox Signal*. 2015; 22(2): 149–60.
9. Hsiao P, Unadkat JD. Predicting the Outer Boundaries of P-glycoprotein (P-gp)-Based Drug Interactions at the Human Blood-Brain Barrier Based on Rat Studies. *Mol Pharm*. 2014; 11(2): 436–44.
10. Yang K, Banerjee S, Proweller A. Regulation of pre-natal circle of Willis assembly by vascular smooth muscle Notch signaling. *Dev Biol*. 2013; 381(1): 107–20.
11. Abbott NJ. Blood-brain barrier structure and function and the challenges for CNS drug delivery. *J Inher Metab Dis*. 2013; 36(3): 437–49.
12. Krueger M, Härtig W, Reichenbach A, et al. Blood-brain barrier breakdown after embolic stroke in rats occurs without ultrastructural evidence for disrupting tight junctions. *PLoS One*. 2013; 8(2): e56419.
13. Lin WY, Chang YC, Ho CJ, et al. Ischemic preconditioning reduces neurovascular damage after hypoxia-ischemia via the cellular inhibitor of apoptosis 1 in neonatal brain. *Stroke*. 2013; 44(1): 162–9.
14. Frontczak-Baniewicz M, Sulejczak D, Andrychowski J, et al. Morphological evidence of the beneficial role of immune system cells in a rat model of surgical brain injury. *Folia Neuropathol*. 2013; 51(4): 324–32.

15. Kim JH, Byun HM, Chung EC, et al. Loss of Integrity: Impairment of the Blood-brain Barrier in Heavy Metal-associated Ischemic Stroke. *Toxicol Res.* 2013; 29(3): 157–64.
16. Alves JL. Blood-brain barrier and traumatic brain injury. *J Neurosci Res.* 2014; 92(2): 141–7.
17. Jackman K, Kunz A, Iadecola C. Modeling focal cerebral ischemia *in vivo*. *Methods Mol Biol.* 2011; 793: 195–209.
18. Rousset E, Kriz J, Seidah NG. Mouse model of intraluminal MCAO: cerebral infarct evaluation by cresyl violet staining. *J Vis Exp.* 2012; 6(69): pii 4038.
19. Winters A, Taylor JC, Ren M, et al. Transient focal cerebral ischemia induces long-term cerebral vasculature dysfunction in a rodent experimental stroke model. *Transl Stroke Res.* 2012; 3(2): 279–85.
20. Lu Z, Zhang W, Jiang S, et al. Effect of oxygen tensions on the proliferation and angiogenesis of endometriosis heterograft in severe combined immunodeficiency mice. *FertilSteril.* 2014; 101(2): 568–76.
21. Qin K, Li YH, Tian G, et al. A much convenient and economical method to harvest a great number of microglia. *Cell MolNeurobiol.* 2012; 32(1): 67–75.
22. Castilla-Ortega E, Rosell-Valle C, Pedraza C, et al. Voluntary exercise followed by chronic stress strikingly increases mature adult-born hippocampal neurons and prevents stress-induced deficits in 'what-when-where' memory. *Neurobiol Learn Mem.* 2013; 109C: 62–73.
23. Armato U, Chakravarthy B, Pacchiana R, et al. Alzheimer's disease: an update of the roles of receptors, astrocytes and primary cilia (review). *Int J Mol Med.* 2013; 31(1): 3–10.
24. Verity MA. Oxidative damage and repair in the developing nervous system. *Neurotoxicology.* 1994; 15(1): 81–91.
25. Ogundele OM, Omoaghe AO, Ajonijebu DC, et al. Glia activation and its role in oxidative stress. *Metab Brain Dis.* 2014; 29(2): 483–93.
26. Osuntokun BO. Cassava diet, chronic cyanide intoxication and neuropathy in the Nigerian Africans. *World Rev Nutr Diet.* 1981; 36: 141–73.
27. Bhattacharya R, Rao P, Singh P, et al. Biochemical, oxidative and histological changes caused by sub-acute oral exposure of some synthetic cyanogens in rats: ameliorative effect of α -ketoglutarate. *Food ChemToxicol.* 2014; 67201–11.
28. United States Environmental Protection Agency (USA-EPA). *Methods for the determination of inorganic substances in environmental samples.* Washington, DC, United States Environmental Protection Agency, Office of Research and Development. 1993; EPA/600/R-93/100.
29. Kristian T, Hu B. Guidelines for using mouse global cerebral ischemia models. *TranslStroke Res.* 2013; 4(3): 343–50.
30. Loenneke JP, Thiebaut RS, Fahs CA, et al. Effect of cuff type on arterial occlusion. *ClinPhysiolFunct Imaging.* 2013; 33(4): 325–5.
31. Nakase H, Heimann A and Kempfski O. Local Cerebral Blood Flow in a Rat Cortical Vein Occlusion Model (1996). *Journal of Cerebral Blood Flow & Metabolism.* 1996; 16: 720–728.
32. Weir-McCall JR, Khan F, Lambert MA, et al. Common carotid intima media thickness and ankle-brachial pressure index correlate with local but not global atheroma burden: a cross sectional study using whole body magnetic resonance angiography. *PLoS One.* 2014; 9(6): e99190.
33. Going JJ. Efficiently estimated histologic cell counts. *Hum Pathol.* 1994; 25(4): 333–6.
34. Kahle MP, Bix GJ. Neuronal restoration following ischemic stroke: influences, barriers, and therapeutic potential. *Neurorehabil Neural Repair.* 2013; 27(5): 469–78.
35. Chu M, Hu X, Lu S, et al. Focal cerebral ischemia activates neurovascular restorative dynamics in mouse brain. *Front Biosci (Elite Ed).* 2012; 4: 1926–36.
36. Rosa AI, Gonçalves J, Cortes L, et al. The angiogenic factor angiopoietin-1 is a proneurogenic peptide on subventricular zone stem/progenitor cells. *J Neurosci.* 2010; 30(13): 4573–84.
37. Rosell A, Moranchó A, Navarro-Sobrino M, et al. Factors secreted by endothelial progenitor cells enhance neurorepair responses after cerebral ischemia in mice. *PLoS One.* 2013; 8(9): e73244.
38. Robertson JM. Astrocytes and the evolution of the human brain. *Med Hypotheses.* 2014 ;82(2)236-9.
39. Umbrello M, Dyson A, Bollen Pinto B, et al. Short-term hypoxic vasodilation *in vivo* is mediated by bioactive nitric oxide metabolites, rather than free nitric oxide derived from haemoglobin-mediated nitrite reduction. *J Physiol.* 2014; 592(Pt 5): 1061–75.
40. Block L, Björklund U, Westerlund A, et al. A new concept affecting restoration of inflammation-reactive astrocytes. *Neuroscience.* 2013; 250536-45.
41. Brambilla R, Morton PD, Ashbaugh JJ, et al. Astrocytes play a key role in EAE pathophysiology by orchestrating in the CNS the inflammatory response of resident and peripheral immune cells and by suppressing remyelination. *Glia.* 2014; 62(3): 452–67.
42. Navarro A, Boveris A, Bández MJ, et al. Human brain cortex: mitochondrial oxidative damage and adaptive response in Parkinson disease and in dementia with Lewy bodies. *Free RadicBiol Med.* 2009; 46(12): 1574–80.
43. Mlynash M, Buckwalter MS, Okada A, et al. Serum neuron-specific enolase levels from the same patients differ between laboratories: assessment of a prospective post-cardiac arrest cohort. *Neurocrit Care.* 2013; 19(2): 161–6.
44. Martínez-Morillo E, GarcíaHernández P, et al. Identification of Novel Biomarkers of Brain Damage in Patients with Hemorrhagic Stroke by Integrating Bioinformatics and Mass Spectrometry-Based Proteomics. *J Proteome Res.* 2014; 13(2): 969–81.
45. Bharosay A, Bharosay VV, Varma M, et al. Correlation of Brain Biomarker Neuron Specific Enolase (NSE) with Degree of Disability and Neurological Worsening in Cerebrovascular Stroke. *Indian J Clin Biochem.* 2012; 27(2): 186–90.
46. Sanchez-de-Toledo J, Chrysostomou C, Munoz R, et al. Cerebral Regional Oxygen Saturation and Serum Neuromarkers for the Prediction of Adverse Neurologic Outcome in Pediatric Cardiac Surgery. *Neurocrit Care.* 2014; 21(1): 133–9.
47. Amorino GP, Parsons SJ. Neuroendocrine cells in prostate cancer. *Crit Rev EukaryotGene Expr.* 2004; 14(4): 287–300.
48. Böhmer AE, Oses JP, Schmidt AP, et al. Neuron-specific enolase, S100B, and glial fibrillary acidic protein levels as outcome predictors in patients with severe traumatic brain injury. *Neurosurgery.* 2011; 68(6): 1624–30; discussion 1630–1.